

Proactive Intra-GPU Disaggregation of Prefill and Decode in LLM Serving

Xiaoxiang Shi*
lambda7xx@gmail.com
Independent Researcher

Colin Cai*
cai9@berkeley.edu
Independent Researcher

Junjia Du
junjia001@e.ntu.edu.sg
Nanyang Technological University

Abstract

Monolithic serving with chunked prefill improves GPU utilization by batching prefill and decode together but suffers from fine-grained phase interference. Engine-level¹ prefill-decode (PD) disaggregation avoids interference but incurs more hardware and high coordination overhead. Prior Intra-GPU disaggregation multiplexes prefill and decode within a single GPU, which uses SLO-based tuning via heuristics derived from offline profiling or feedback loop to allocate GPU resource but respond reactively to performance issues rather than anticipating them, limiting the ability to adapt efficiently under dynamic workloads.

We ask: can we achieve proactive Intra-GPU disaggregation that adapts effectively to dynamic workloads? The key challenge lies in managing the conflicting resource demands of prefill and decode under varying workload conditions. In this paper, we first show that GPU resources exhibit diminishing returns—beyond a certain saturation point, increasing allocation provides minimal latency benefits. Second, we observe that under dynamic workloads, memory bandwidth contention becomes a critical performance bottleneck. These insights motivate a design that splits a single GPU’s resources and dynamically allocates them between prefill and decode phases, while jointly considering compute capacity, memory footprint, and bandwidth contention

Evaluated across diverse LLMs and workloads, our system Nexus achieves up to **2.2 \times** higher throughput, **20 \times** lower TTFT, and **2.5 \times** lower TBT than vLLM; outperforms SGLang by up to **2 \times** ; and matches or exceeds the performance of disaggregated vLLM while using only half the GPU resources.

1 Introduction

Transformer-based [54] Large Language Models (LLMs) [4, 11, 18, 41] have achieved state-of-the-art performance on a wide range of tasks, from natural language understanding to code synthesis [2, 19, 20, 27, 29, 40, 51, 58, 59]. The success has also driven their integration into latency-sensitive applications such as chatbots [11, 18, 19, 40, 41, 51], search assistants [44], and AI-augmented IDEs [10]. In interactive settings, even small delays matter a lot: humans perceive latencies above one second as disruptive [67], and sub-second

*Both authors contributed equally to this work.

¹We use the term *engine* to denote a unit of GPUs that manages exactly one complete copy of the model weights.

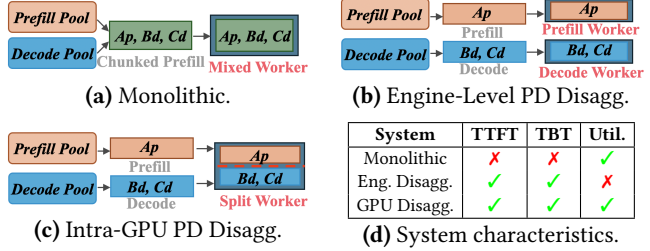


Figure 1. Design evolution of LLM inference systems. Comparison between monolithic, engine-level disaggregated, and intra-GPU disaggregated designs. Ap is the prefill phase of request A; Bd, Cd, and Dd are the decode phases of requests B, C, and D.

improvements has been shown to substantially boost engagement [16]. Therefore, latency is a critical performance metric for LLM serving.

LLM inference consists of two distinct stages with heterogeneous resource demands: *prefill* and *decode*. In the prefill stage, the model processes the entire prompt in a single forward pass to populate the key-value (KV) cache and produce the first output token. This stage is typically *compute-bound* [42, 68], dominated by large matrix multiplications that fill GPU compute units. In contrast, the decode stage generates tokens one at a time, attending to all previously cached KV states. The decode stage features lightweight compute but requires reading the full model weights and the entire KV cache, making it heavily constrained by memory bandwidth [24, 25, 42, 68].

These two stages naturally give rise to two critical latency metrics in LLM serving: *time-to-first-token (TTFT)*, the delay before the first output token is produced, determined by prefill; and *Time-between-Tokens (TBT)*, the latency between subsequent tokens, dictated by the decode loop. These metrics directly impact the user experience in latency sensitive applications. Optimizing TTFT and TBT has driven a wave of innovations in LLM serving systems, spanning scheduling, batching, and kernel design [1, 15, 24, 25, 30–33, 39, 50, 56, 57, 61, 63, 64, 66, 67].

Conventional LLM serving systems fall into two broad classes based on placement of prefill and decode (Figure 1a, 1b).

Monolithic systems [1, 25, 30, 52, 63, 66, 68] execute both stages within a single engine. To improve utilization, recent designs like Sarathi-Serve [1] adopt *chunked prefill*, where long prompts are split into shorter chunks and batched alongside decode tokens on the same device. This increases batch

efficiency and improves token throughput. However, it mixes compute heavy prefill and memory sensitive decode in the same batch, causing interference (see Section 3.1).

Engine-Level PD Disaggregated systems [23, 42, 45, 67] assign prefill and decode to separate engines, transferring KV cache data between them. This eliminates interference and consistently achieves low TTFT and TBT. But it sacrifices efficiency: decode engines are often underutilized, and multi-GPU deployment incurs additional hardware and communication overhead, especially when KV state is large [15, 22].

Motivated by these limitations and enabled by growing GPU capacity [34, 36], recent systems have begun to explore *intra-GPU PD disaggregation* (Figure 1c), running prefill and decode concurrently within a single GPU via spatial or temporal multiplexing [9, 22, 26]. These systems demonstrate the feasibility of intra-GPU disaggregation and show isolating phases within a single device can yield performance benefits.

However, existing solutions guide resource allocation using offline profiling, simple inverse-scaling models, or latency-driven control loops. While these approaches can be effective under stable SLOs or predictable traffic, they lack the adaptability required to respond to changing prompt lengths, KV Cache sizes, and evolving batch compositions. Critically, they fail to jointly model the three core resource pressures: compute saturation, memory bandwidth contention, and runtime memory usage. As a result, these systems adjust resource allocations only after detecting latency violations, making them reactive rather than proactive. This passivity limits their ability to anticipate interference and proactively prevent performance collapse under shifting workloads.

These challenges call for a runtime system that can model such dynamics explicitly, and proactively adapt resource allocation and scheduling within sub-second granularity. We present *Nexus*, a monolithic LLM serving engine that performs intra-GPU PD disaggregation through model-guided scheduling and lightweight per-batch optimization.

Nexus is built on three components: (1) A contention-aware cost model that predicts latency as a function of compute saturation and memory interference. It is parameterized by a lightweight one-time kernel profiling pass per configuration and requires no workload-specific retraining or online feedback tuning. The model feeds into a dual-objective optimization routine with relaxed latency constraints, solved via fast greedy search to determine per-batch SM partitioning. (2) A buffered asynchronous switching mechanism that mitigates instability during SM reallocation by introducing a hysteresis zone. This avoids oscillation from transient workload shifts and ensures smooth partition transitions. (3) Two phase-specific schedulers: a Shortest-Prompt-First (SPF) policy for prefill to minimize TTFT under skewed prompt lengths, and a simple FCFS policy for decode to preserve fairness and responsiveness.

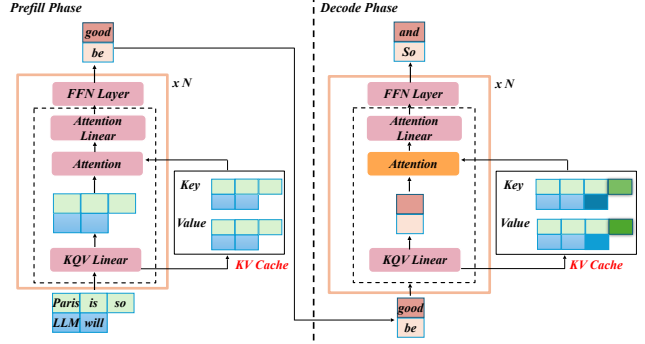


Figure 2. Inference process of transformer-based LLMs. Red boxes indicate compute-bound operations (KQV Linear, Prefill Attention, Attention Linear, and FFN Layer), while the orange box (Attention) represents a memory-bound operation. Auxiliary components such as LayerNorm are omitted for clarity.

We implement *Nexus* by extending vLLM [25] with fine-grained SM partitioning and concurrent prefill-decode execution. *Nexus* runs on commodity GPUs, supports decoder-only LLMs, and requires no specialized hardware.

This paper makes the following contributions:

- We identify diminishing compute returns and phase-dependent memory bandwidth contention as key system level bottlenecks in intra-GPU LLM serving.
- We develop a lightweight, contention-aware runtime framework that models these effects analytically and solves a dual-objective GPU allocation problem via fast greedy search without relying on workload-specific profiling or SLO feedback.
- We implement *Nexus* as a drop-in vLLM extension and evaluate it on production-scale LLMs and traffic. *Nexus* achieves up to $2.2\times$ and $2\times$ higher throughput, $20\times$ and $2\times$ lower TTFT, and $2.5\times$ and $1.7\times$ lower TBT than vLLM and SGLang respectively, and outperforms disaggregated vLLM with half the GPU resources.

2 Background

2.1 Architecture of Transformer-based LLM

Most large language models (LLMs) [3, 5, 14] adopt a decoder-only Transformer architecture [54], consisting of a stack of layers that apply self-attention and feed-forward networks (FFNs). During inference, LLMs operate in two distinct phases: *prefill* and *decode*. Figure 2 illustrates the computation involved in each phase. The left panel depicts the prefill phase, where the prompt is processed to produce the first token and KV cache. The right panel shows the decode phase, where tokens are generated autoregressively using the cached KV states. Each Transformer layer includes both attention-related operations and dense operations [68]. The latter consist of the linear projections for queries, keys, and values (Q/K/V), the output projection following attention,

and the FFN sublayer. All these dense operations are compute bound [42, 68].

2.2 Dense Operations

Q/K/V Projections. Before attention, the input X is projected by weight matrices W_Q , W_K , and W_V to produce the corresponding Query, Key, and Value tensors. $W_Q, W_K, W_V \in \mathbb{R}^{d \times d}$ where d is the hidden size.

$$Q = XW_Q, \quad K = XW_K, \quad V = XW_V \quad (1)$$

Without caching, all L tokens are processed, leading to $O(Ld^2)$ compute. With caching, only the n new tokens require projection, reducing the cost to $O(nd^2)$.

Attention Output Projection. The attention output $A \in \mathbb{R}^{n \times d}$ is projected using:

$$O = AW_O, \quad W_O \in \mathbb{R}^{d \times d} \quad (2)$$

The cost is $O(nd^2)$, or $O(Ld^2)$ if no caching is used.

Feed-Forward Network (FFN). Each token is independently processed by a two-layer MLP with a non-linear activation (typically GELU):

$$\text{FFN}(x) = \text{GELU}(xW_1 + b_1)W_2 + b_2 \quad (3)$$

where $W_1 \in \mathbb{R}^{d \times d_{\text{ff}}}$, $W_2 \in \mathbb{R}^{d_{\text{ff}} \times d}$, and typically $d_{\text{ff}} = 4d$. The cost is $O(nd \cdot d_{\text{ff}})$, or $O(Ld \cdot d_{\text{ff}})$ in the absence of caching. Given the size of d_{ff} , this is usually the most FLOP-intensive component of the layer.

2.3 Attention Operation

Self-attention computes token-level dependencies by comparing queries with keys and applying attention weights to values. Given query $Q \in \mathbb{R}^{n \times d}$, key $K \in \mathbb{R}^{L \times d}$, and value $V \in \mathbb{R}^{L \times d}$, attention is computed as:

$$S = \frac{QK^\top}{\sqrt{d}}, \quad A = \text{softmax}(S)V, \quad A \in \mathbb{R}^{n \times d} \quad (4)$$

The attention computation has two main components: - Computing similarity scores $S \in \mathbb{R}^{n \times L}$: cost $O(nLd)$, - Applying softmax and aggregating over values: cost $O(nLd)$.

Thus, the overall attention complexity is $O(nLd)$. In the absence of KV caching, this becomes $O(L^2d)$.

Prefill vs. Decode Attention. Assuming cache is enabled, the difference between prefill and decode arises from the size of n . In the *prefill phase*, a chunk of n new tokens is processed in parallel. The attention computation involves matrix-matrix multiplications and has cost $O(nLd)$, which is compute-bound [68] and benefits from parallelism. In the *decode phase*, only one new token is processed at a time ($n = 1$), resulting in a matrix-vector multiplication (GEMV) with cost $O(Ld)$. While the FLOP count is low, this operation is memory-bound [68] due to repeated access to the model weights and the growing KV cache.

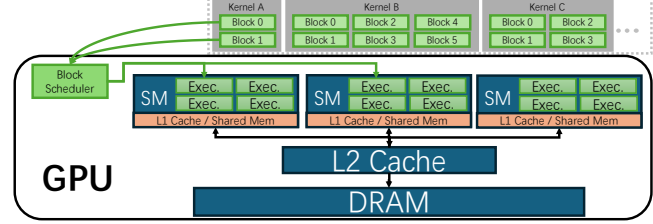


Figure 3. Simplified GPU execution model. Modern GPUs share a global kernel queue, with SMs (streaming multiprocessors) dynamically fetching kernels to execute. Concurrently executing kernels compete for shared memory bandwidth.

These contrasting patterns lead to different system bottlenecks [24, 25]: prefill benefits from parallelism, while decode demands cache-efficient execution.

2.4 Batching in LLM Serving

LLM serving systems batch requests to improve throughput by maximizing GPU utilization. However, batching must account for two distinct stages of execution: *prefill*, which processes the full input prompt and is compute-heavy and batch-friendly; and *decode*, which generates one token at a time and is memory-bound, latency-sensitive, and harder to parallelize. These phases differ in resource demand and can interfere when co-scheduled on the same GPU, motivating a spectrum of batching and disaggregation strategies.

We categorize prior designs based on how they separate or interleave prefill and decode execution:

Monolithic Systems. Monolithic system [25, 66] such as Sarathi-Serve [1] (Figure 1a) splits long prompts into fixed-size chunks and mixing them with decode tokens in a shared batch queue. These systems construct mixed-phase batches that improve GPU utilization and reduce head-of-line blocking.

Engine-Level PD Disaggregation. To isolate prefill and decode execution, some systems adopt engine-level prefill-decode disaggregation [23, 42, 45, 67] (Figure 1b), assigning each phase to separate serving engine. This strategy enables independent scheduling and eliminates interference between prefill and decode, particularly in multi-GPU environments.

Intra-GPU PD Disaggregation. A newer class of systems [9, 22, 26] disaggregates prefill and decode within a single GPU. These systems aim to combine the efficiency of monolithic designs with the phase isolation of disaggregated ones. They typically rely on latency-targeted orchestration, offline profiling, or isolation-based scheduling. Our work follows this line of design but focuses on model-driven, fine-grained proactive scheduling to enable per-batch adaptation.

2.5 GPU Execution Model

Modern LLM inference relies heavily on GPU acceleration. Figure 3 presents a simplified view of GPU execution, abstracting low-level scheduling mechanisms in favor of architectural components most relevant to LLM serving workloads.

GPUs consist of multiple Streaming Multiprocessors (SMs), each with its own block executor, L1 cache, and register file, while sharing a unified L2 cache and off-chip DRAM. Kernels are submitted via a global software queue and consists of many blocks. The blocks carry operations and are scheduled onto available executors in SMs by a hardware-level scheduler, which is largely opaque to software and does not provide preemptive control or fine-grained prioritization.

GPU Multiplexing. Modern GPUs support spatial multiplexing via three main mechanisms: NVIDIA MPS, MIG, and CUDA GreenContext [35, 37, 38]. MPS allows concurrent kernel execution across processes with partial SM sharing, while MIG enforces strict hardware-level SM partitioning with fixed memory allocations. GreenContext enables logical SM isolation within a single GPU process by assigning execution streams to non-overlapping SM sets if resource permits. While these mechanisms offer fine-grained compute isolation, they do not virtualize memory bandwidth: all SM partitions share the same L2 cache and DRAM channels. Thus, concurrent execution of kernels can still suffer from contention on the memory subsystem, degrading performance.

3 Motivation

Modern LLM serving must coordinate two asymmetric phases: compute-heavy *prefill* [42, 68] and memory-bound, latency-sensitive *decode* [24, 25, 42, 68]. These phases contend for GPU resources in different ways, complicating scheduling and batching decisions.

In this section, we examine the limitations of existing systems that either mix or isolate these phases (§3.1); demonstrate how both prefill and decode exhibit diminishing returns under increased compute allocation (§3.2); and show that static GPU partitioning fails to account for dynamic memory contention that emerges at runtime (§3.3). Together, these observations motivate the need for a runtime system that can adaptively allocate GPU resources while explicitly accounting for compute saturation and memory bandwidth interference.

Setup. Unless otherwise stated, we evaluate using the Long Data Collections workload (§6.1) on Qwen2.5–3B running on a single NVIDIA L20 GPU. Requests arrive via a Poisson process at 2.5 req/s. We use NVIDIA MPS [38] to enforce strict SM partitioning.

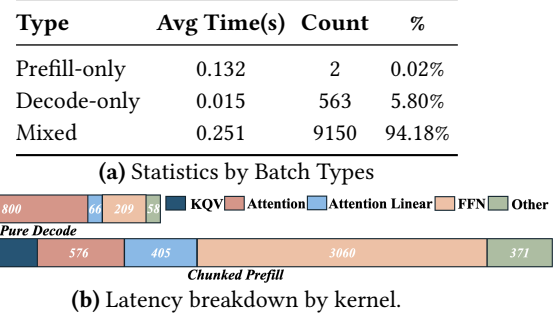


Figure 4. Latency impact of mixed prefill–decode batches. (a) Prefill-only and decode-only batches have predictable latency, but mixed batches cause 8×–10× slowdown due to interference. (b) Kernel-level profiling reveals that even lightweight decode kernels experience inflated runtimes when co-executed with prefill. This highlights the fine-grained contention caused by chunked batching.

3.1 Limitation of Existing Solutions

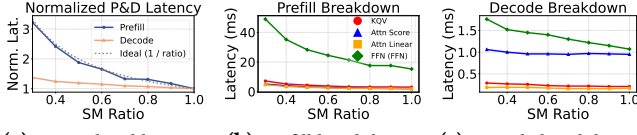
Modern LLM serving systems adopt three high-level strategies to manage prefill and decode execution: *monolithic batching*, *engine-level disaggregation*, and *intra-GPU disaggregation*. While each aims to mitigate resource contention between compute-heavy prefill and latency-sensitive decode, they introduce trade-offs that limit flexibility and efficiency.

Monolithic Systems. Monolithic systems [1, 25, 63, 66] batch prefill and decode requests together, often using chunked prefill to improve utilization. However, this co-scheduling introduces interference between resource-asymmetric stages. We categorize batches into *prefill-only*, *decode-only*, and *mixed*, and measure their iteration times (Figure 4a). Despite having similar token counts, mixed batches average 250 ms, compared to just 15 ms for decode-only batches.

This slowdown arises from prefill computation (e.g., KQV projection, FFN) blocking lightweight decode kernels within a batch. As shown in Figure 4b, decode kernel latency increases up to 10× when co-scheduled with prefill, inflating TBT by more than 8×.

Engine-Level Disaggregation. Engine-level disaggregation [42, 45, 67] assigns prefill and decode to separate GPU engines, eliminating phase interference. While this stabilizes latency, it incurs steep hardware and coordination costs: model replication, underutilized decode engines, and KV-cache transfer overhead. These systems also assume fixed phase placement and lack runtime adaptation. Under bursty or decode-heavy conditions, coordination failures can trigger cache eviction, recomputation, or out-of-memory (OOM) errors (§6.2.2) [15, 22].

Intra-GPU Disaggregation. Recent systems such as Bullet [26], Drift [9], and semi-PD [22] disaggregate prefill and decode execution within a single GPU, reducing hardware cost and avoiding cross-GPU KV transfers. These designs demonstrate that intra-GPU disaggregation is feasible, but often rely on simplified assumptions. Bullet uses SLO-guided



(a) Normalized latency. (b) Prefill breakdown. (c) Decode breakdown.

Figure 5. Diminishing returns in prefill and decode with increasing SM allocation. (a) End-to-end latency for prefill and decode flattens well before full SM usage. (b) Prefill kernels (e.g., FFN, KQV, attention linear) show varied sensitivity to SM scaling, with FFN benefiting the most. (c) Decode kernels saturate quickly, confirming that decode is memory-bound and gains little from additional compute.

feedback to adjust resource allocations based on profile-derived latency estimators. Drift assumes contention-free execution and applies gang scheduling with phase tagging. Semi-PD fits inverse-scaling latency models and applies windowed feedback to guide SM partitioning. While effective under predictable workloads, these methods are inherently reactive and do not explicitly model two critical system-level factors: (1) diminishing returns in compute allocation, and (2) dynamic memory bandwidth contention. As we show in the next sections, both effects vary significantly across phases and should be anticipated to enable robust, fine-grained adaptation.

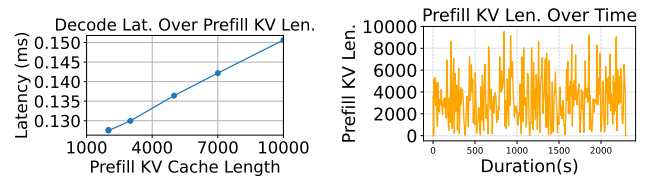
3.2 Diminishing Returns in Compute Allocation

To guide effective GPU resource allocation between prefill and decode, we begin by analyzing how each phase scales with compute in isolation. We run pure prefill and decode batches under varying SM ratios, measuring both end-to-end latency and per-kernel runtimes.

As shown in Figure 5, prefill latency follows the expected scaling curve $T \propto \frac{1}{r}$, with diminishing returns emerging gradually. For example, increasing SM allocation from 30% to 40% reduces latency by over 25%, but this gain drops to 10% when increasing from 70% to 80%. A breakdown in Figure 5b shows that compute-heavy layers such as FFN continue to benefit from more SMs, while others like KQV and projection flatten earlier at 60%.

Decode exhibits sharper diminishing returns. Increasing SMs from 30% to 40% yields only a 10% latency reduction, and beyond 50%, further increases offer less than 3% improvement per 10% step. This behavior aligns with the decode phase being memory-bound and less compute-scalable. As shown in Figure 5c, attention and projection kernels see minimal speedup.

These trends highlight a critical asymmetry: prefill and decode have different compute saturation points. Instead of time-slicing all SMs between the two stages, it is more efficient to spatially partition resources, assigning only what each phase needs. Engine-Level Disaggregated systems, which dedicate full GPUs to each phase, often operate in high regions of diminishing returns.



(a) Impact of prefill KV length on (b) Observed variation in prefill decode latency. KV length during execution.

Figure 6. Memory contention's impact and variability. (a) Decode latency increases as prefill KV length grows due to shared memory bandwidth pressure; (b) Prefill KV length fluctuates significantly over time, making contention difficult to predict statically.

Insight 1. Both prefill and decode saturate well before full GPU allocation. To avoid overprovisioning, systems should allocate only the SMs needed to meet each phase's demand. These compute asymmetries motivate analytical modeling that accounts for per-kernel scaling to guide partitioning.

3.3 Limitation of Static Partitioning

Section 3.2 shows that prefill and decode exhibit diminishing returns with increasing SM allocation, motivating phase-aware compute partitioning. However, even a well-chosen *static* partition is insufficient in practice. This is because compute demand, while often estimable from inputs like chunk size or sequence length, does not account for dynamic memory behavior during serving. Prefill and decode phases contend for memory bandwidth in ways that depend on runtime factors such as evolving KV-cache sizes, prompt distributions, and decode lengths.

To illustrate this, we co-execute prefill chunks² with pure decode batches under a fixed SM partition. As shown in Figure 6a, increasing the prefill KV length from 2,000 to 10,000 increases decode latency by 36%, despite the decode workload itself remaining constant. This slowdown stems from bandwidth contention: prefill attention layers issue large KV reads that overlap with latency-critical memory accesses from the decode phase.

Figure 6b further shows that prefill memory traffic is highly irregular and fluctuates significantly over time, making contention both unpredictable and workload-dependent.

These results highlight a fundamental limitation: even when compute needs are analyzable, memory bandwidth pressure can vary rapidly due to asynchronous phase behavior. Static SM partitioning cannot react to this dynamic interference, leading to resource underutilization and inflated latency.

²Following Sarathi-Serve [1], long prompts are split into smaller segments and processed alongside decode requests. These prefill chunks actively read and write to the KV cache.

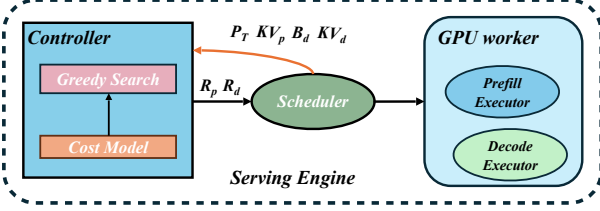


Figure 7. System architecture of Nexus. R_p and R_d denote the SM ratios allocated to prefill and decode, respectively. P_T represents the chunk prompt length of prefill, KV_p is the total KV cache used during prefill, B_d is the decode batch size, and KV_d is the total KV cache used during decoding.

Insight 2. Intra-GPU PD disaggregation with static resource allocation is insufficient under dynamic memory contention. Effective intra-GPU scheduling requires runtime-aware, fine-grained SM reallocation that adapts to emergent phase interference.

4 Design

We present Nexus, a lightweight monolithic LLM serving system that enables *intra-GPU prefill-decode disaggregation* through proactive SM partitioning and phase-aware scheduling. Unlike reactive systems that adjust only after SLO violations, Nexus proactively predicts performance bottlenecks using a contention-aware cost model and dynamically reallocates resources in real time. This enables high utilization without introducing interference. As shown in Figure 7, Nexus introduces three core mechanisms to enable this fine-grained separation:

- **Dynamic SM Partitioning** (§4.1): A runtime cost model estimates per-phase iteration latency based on compute scaling and memory contention. We formalize a dual-objective optimization problem and solve it efficiently via a greedy search.
- **Stability Control** (§4.2): To reduce the overhead of frequent re-partitioning, we apply a hysteresis-style buffer zone that filters out insignificant SM ratio changes.
- **Phase-Specific Scheduling** (§4.3): With prefill and decode isolated, we deploy customized schedulers to optimize TTFT and TBT jointly.

These components form a closed-loop control system that continuously adapts GPU resource allocation to match workload demands, preserving high utilization without reintroducing interference.

4.1 Dynamic SM Partitioning via Cost Model

To execute prefill and decode concurrently without introducing significant interference or wasting resources, Nexus must decide at runtime how to split GPU computes between the two phases. This is challenging: exhaustive search is too

slow for inference loops, and simple rules fail under dynamic memory contention.

To solve this, Nexus combines three components: (1) an analytical cost model that predicts latency under any SM split, (2) a dual-mode optimization objective that shifts focus based on runtime signals, and (3) a greedy search algorithm that efficiently selects SM partitions with just a few cost model queries.

4.1.1 Cost Model. Nexus’s cost model estimates the latency of prefill and decode under SM allocations without execution. This avoids reliance on feedback-based tuning or runtime latency profiling, and supports proactive, per-batch optimization not possible in prior reactive systems.

Each iteration consists of multiple operators with different bottlenecks. For example FFNs are compute-bound [68], while a decode attention may be memory-bound [68] as KV grows. These characteristics shift with workload, so we model each phase’s latency as a sum over operators:

$$T_{\text{prefill}} = \sum_{i \in \text{PrefillOps}} \max(T_i^{\text{compute}}, T_i^{\text{mem}}) \quad (5)$$

$$T_{\text{decode}} = \sum_{j \in \text{DecodeOps}} \max(T_j^{\text{compute}}, T_j^{\text{mem}}) \quad (6)$$

This operator-level modeling captures shifting bottlenecks, such as decode attention flipping between compute- and memory-bound, without collapsing structure as coarse stage-level models would.

Compute Latency. We estimate the compute latency of each operator $o \in \text{PrefillOps} \cup \text{DecodeOps}$ based on its FLOP count c_o and the SM ratio r assigned to its stage. While latency ideally scales inversely with compute share ($1/r$), real-world performance can deviate depending on the kernel (§3.2).

To model this, we use a two-regime saturation-decay curve

- *Sub-saturation*: Latency scales near-inversely with r until a saturation threshold R_{sat} ;
- *Post-saturation*: Additional SMs yield diminishing returns, modeled by a decay coefficient λ .

$$T_o^{\text{compute}}(c_o, r) = \begin{cases} \frac{c_o}{r \cdot C} & \text{if } r \leq R_{\text{sat}} \\ \frac{c_o}{R_{\text{sat}} \cdot C} \cdot (1 + \lambda \cdot (r - R_{\text{sat}})) & \text{otherwise} \end{cases} \quad (7)$$

where C is the peak throughput of the GPU.

These coefficients (R_{sat}, λ) are extracted from a one-time profiling pass per model, avoiding the need for runtime latency fitting and transferable across workloads.

Memory Contention Aware Model. As shown in §3.3, memory contention can significantly affect latency when prefill and decode execute concurrently on shared hardware. Unlike prior work that ignores phase overlap or assumes

fixed latency models, we model decode attention latency as a function of runtime overlap with memory-bound prefill activity and the relative memory bandwidth during contention.

Let T_{prefill} denote total prefill duration, and $T_{\text{prefill}}^{\text{attn}}$ be the estimated time on memory-bound attention layers. Then the probability that decode overlaps with prefill attention is:

$$P_{\text{attn}} = \frac{T_{\text{prefill}}^{\text{attn}}}{T_{\text{prefill}}} \quad (8)$$

We conservatively assume that prefill's dense layers consume memory bandwidth during the remaining time, yielding:

$$P_{\text{dense}} = 1 - P_{\text{attn}}$$

Assuming full bandwidth saturation during each overlap window, we allocate effective bandwidth to decode based on its share of memory traffic. Let m_d be the total memory bytes accessed by decode attention, m_{p1} the bytes accessed by prefill attention, and m_{p2} those accessed by prefill's dense operators.³ Then the effective bandwidth for decode is:

$$B_{\text{decode}} = \frac{m_d}{m_d + m_{p1}} \cdot P_{\text{attn}} \cdot B + \frac{m_d}{m_d + m_{p2}} \cdot (1 - P_{\text{attn}}) \cdot B$$

Decode memory latency is then computed as:

$$T_{\text{decode}}^{\text{mem}} = \frac{m_d}{B_{\text{decode}}} \quad (9)$$

This formulation captures two important dynamics: (1) contention grows with total memory traffic, reducing effective bandwidth; (2) allocating more SMs to decode slows prefill (via compute contention), stretching T_{prefill} , which reduces P_{attn} and mitigates contention. This feedback is integrated into the overall cost model and guides SM partitioning decisions.

While decode involves multiple operators, we model memory contention only for attention, which dominates bandwidth usage. Other components are lightweight or compute-bound, and do not significantly impact contention. For prefill, we estimate memory latency assuming peak bandwidth, and use the resulting memory-bound segments only to compute P_{attn} . This separation avoids circular dependencies while capturing the dominant interaction between phases.

4.1.2 Optimization Objective. Given the cost model, Nexus selects an SM partition that balances performance and memory pressure. However, since prefill and decode run concurrently and compete for GPU compute, GPU memory and GPU memory bandwidth, optimizing both simultaneously can lead to inefficient tradeoffs.

To resolve this, Nexus formulates a *dual-objective latency optimization*: prioritize one phase while constraining the

³We estimate memory access volume for linear layers using known parameter sizes from the model architecture. For attention, we weight memory access and calculate KV memory traffic based on the number of cached tokens tracked by vLLM, multiplied by the per-token key/value size determined from model dimensions.

other to remain within a slowdown budget. This allows flexible tradeoffs between TBT and TTFT, depending on workload state. The choice is also guided by runtime signals, such as KV cache usage, to avoid pathological behaviors like OOM or long waiting time.

Formulation. Let $T_{\text{prefill}}(R_p)$ and $T_{\text{decode}}(R_d)$ denote the estimated latencies under a given SM split R_p and $R_d = 1 - R_p$. We define two optimization modes:

- **Decode-prioritized:**

$$\begin{aligned} \min_{R_p} \quad & T_{\text{decode}}(1 - R_p) \\ \text{s.t.} \quad & T_{\text{prefill}}(R_p) \leq \alpha \cdot T_{\text{prefill}}^{\min} \\ & 0 \leq R_p \leq 1 \end{aligned}$$

- **Prefill-prioritized:**

$$\begin{aligned} \min_{R_p} \quad & T_{\text{prefill}}(R_p) \\ \text{s.t.} \quad & T_{\text{decode}}(1 - R_p) \leq \beta \cdot T_{\text{decode}}^{\min} \\ & 0 \leq R_p \leq 1 \end{aligned}$$

Here, T^{\min} denotes the ideal latency when a stage is allocated all SMs, and $\alpha, \beta > 1$ are slack variables controlling tolerable slowdowns in the non-prioritized stage. Unlike SLO thresholds, these slack constraints are batch-dependent and derived from the cost model itself.

Runtime Switching. We select the objective mode based on live KV cache usage KV_u : when KV_u is low, prioritizing prefill improves TTFT by accelerating prompt ingestion. When KV_u is high, prioritizing decode helps reduce memory pressure by completing generation and evicting old KV entries. This feedback mechanism enables resource allocation to respond to workload phases and memory constraints.

$$\text{Objective Mode} = \begin{cases} \text{Prefill-prioritized} & \text{if } KV_u \leq KV_{\text{switch}} \\ \text{Decode-prioritized} & \text{otherwise} \end{cases}$$

This mode-switching behavior is key to handling dynamic workloads. Rather than rely on fixed priorities or static thresholds, Nexus adapts its scheduling objective based on system state, enabling both high throughput and memory safety.

4.1.3 Greedy SM Search. Since prefill and decode iterations run in sub-second times, we do not attempt to globally solve the constrained optimization; instead, we use a two-phase greedy adjustment that is fast, robust, and effective in practice.

Phase 1: Constraint Satisfaction. Starting from the current allocation, the algorithm reduces the SM share of the prioritized stage until the non-prioritized stage's latency constraint is satisfied (lines 21–23 in Algorithm 1).

Phase 2: Target Optimization. Once within the feasible region, the algorithm gradually increases the SM share of

Algorithm 1 Nexus’s SM Partitioning with Greedy Search and Buffer Control

```

1 Input:  $KV_u$ ,  $R_p^{\text{cur}}$ ,  $R_d^{\text{cur}}$ 
2 Output: New partition  $(R_p^{\text{new}}, R_d^{\text{new}})$ 
3 procedure PARTITIONCONTROLLER( $KV_u$ ,  $R_p^{\text{cur}}$ ,  $R_d^{\text{cur}}$ )
4   if  $KV_u > KV_{\text{switch}}$  then
5      $(R_p^{\text{new}}, R_d^{\text{new}}) \leftarrow \text{ADJUSTPARTITION}(\text{decode}, R_p^{\text{cur}}, R_d^{\text{cur}})$ 
6   else
7      $(R_p^{\text{new}}, R_d^{\text{new}}) \leftarrow \text{ADJUSTPARTITION}(\text{prefill}, R_p^{\text{cur}}, R_d^{\text{cur}})$ 
8   end if
   ▷ Buffer zone check to suppress unstable or small changes
9   if  $|R_p^{\text{new}} - R_p^{\text{cur}}| < \delta$  then
10    return  $(R_p^{\text{cur}}, R_d^{\text{cur}})$ 
11   else
12     return  $(R_p^{\text{new}}, R_d^{\text{new}})$ 
13   end if
14 end procedure

15 procedure ADJUSTPARTITION( $\text{target}$ ,  $R_p^{\text{cur}}$ ,  $R_d^{\text{cur}}$ )
16   Let  $\text{other} \leftarrow (\text{target is prefill? decode : prefill})$ 
17   Let  $\text{Slack} \leftarrow (\text{target is prefill? } \beta : \alpha)$ 
18    $T_{\text{other}}^{\text{opt}} \leftarrow \text{COSTMODEL}(\text{other}, 100)$ 
19    $R_{\text{cur}} \leftarrow (\text{target is prefill? } R_p^{\text{cur}} : R_d^{\text{cur}})$ 
20    $R \leftarrow R_{\text{cur}}$ 
   ▷ Phase 1: Decrease until constraint is satisfied
21   while  $\text{COSTMODEL}(\text{other}, 100 - R) > \text{Slack} \cdot T_{\text{other}}^{\text{opt}}$  do
22      $R \leftarrow R - 1$ 
23   end while
   ▷ Phase 2: Increase target share until constraint is at limit
24   while  $R < 100$  do
25      $T_{\text{other}} \leftarrow \text{COSTMODEL}(\text{other}, 100 - (R + 1))$ 
26     if  $T_{\text{other}} > \text{Slack} \cdot T_{\text{other}}^{\text{opt}}$  then
27       break
28     end if
29      $R \leftarrow R + 1$ 
30   end while
31   return  $(\text{target is prefill? } (R, 100 - R) : (100 - R, R))$ 
32 end procedure

```

Note: CostMODEL(phase, R) estimates phase latency under R ; all ratios are expressed as percentages of total SMs; β is tolerance for primary objective’s deviation from optimal; δ is the buffer to avoid frequent switches.

the prioritized stage, improving its latency as long as the constraint remains satisfied (lines 24–30).

Efficiency. We avoid global constrained solvers due to their overhead. Instead, a simple greedy search provides robustness and transparency while converging in just 2–4 iterations. This efficiency is also critical for per-batch decision making during inference.

4.2 Hysteresis-Based SM Repartitioning for Stability

While selecting the optimal SM split is critical for reducing prefill–decode interference, the timing and stability of repartitioning are equally important. Green Contexts provide logical SM isolation, but switching partition states is not

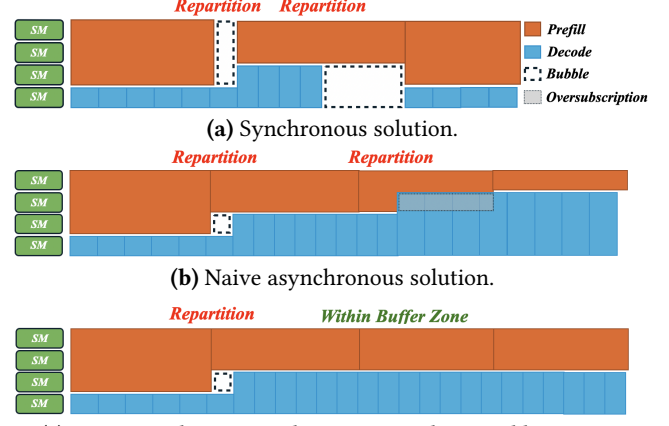


Figure 8. Mechanisms for SM partition switching. Comparison between synchronous, asynchronous, and our asynchronous with hysteresis approach.

free: transitions can introduce temporary underutilization, overcommitment, or execution stalls.

Pitfall 1: Synchronous switching. A natural design is to synchronize partition changes at global checkpoints. However, as shown in Figure 8a, this introduces idle “bubbles,” where some streams stall waiting for others to reach the switch point. It hurts SM utilization and inflates latency.

Pitfall 2: Naive asynchronous switching. Letting streams switch independently avoids global stalls, but creates new problems: SM oversubscription or underutilization depending on timing (Figure 8b). This makes system sensitive to transient workload shifts, causing back-and-forth toggling and instability.

Our design: Buffered asynchronous switching. To mitigate these issues, Nexus adopts a buffered asynchronous switching policy. The runtime controller tracks the last-applied SM ratio and only triggers repartitioning when the new target differs by more than a threshold δ . This hysteresis-style buffer (Figure 8c) smooths out transient fluctuations and suppresses excessive reconfiguration. The logic is embedded in Algorithm 1, line 9–13.

This simple mechanism retains the adaptability of fine-grained decisions while avoiding the instability of overreactive switching. Alternative approaches like naively reducing the update frequency sacrifices responsiveness, while large step sizes risk overshooting optimal ratios. In contrast, our hysteresis design filters out noise and enables smooth SM reallocation under dynamic workloads.

4.3 Phase-Specific Scheduler

Since Nexus separates prefill and decode into concurrent batches, we can further exploit this with phase-specific optimizations. While SM partitioning governs how much resource each phase gets, our schedulers govern how that resource is consumed. Particularly, we employ scheduler

Algorithm 2 Nexus’s Shortest Prompt First (SPF) Scheduler

```

1 Input: Request queue  $Q$ , batch limit  $B$ , age decay factor  $\alpha$ 
2 Output: The next prefill batch to run
3 procedure SPF_SCHEDULE(Queue  $Q$ , Int  $B$ , Float  $\alpha$ )
4   for all  $r \in Q$  do
5      $r.\text{remaining} \leftarrow r.\text{prompt\_len} - r.\text{prefilled\_len}$ 
6      $r.\text{score} \leftarrow r.\text{remaining} - \gamma \cdot r.\text{age}$   $\triangleright$  Antistarvation
7   end for
8    $Q_{\text{sorted}} \leftarrow \text{SORTBY}(Q, r \mapsto r.\text{score})$ 
9    $batch \leftarrow []$ 
10   $total \leftarrow 0$ 
11  for  $r \in Q_{\text{sorted}}$  do
12    if  $total + r.\text{remaining} \leq B$  then
13      APPEND( $batch, r$ )
14       $total \leftarrow total + r.\text{remaining}$ 
15    else
16      break
17    end if
18  end for
19  return  $batch$ 
20 end procedure

```

policies tailored to the latency and compute characteristics of each phase.

4.3.1 Prefill Scheduler. TTFT is governed by the prefill stage, which must complete a full forward pass before emitting output. When scheduling prompt requests of varying lengths, naïve policies can introduce head-of-line (HoL) blocking: short prompts are delayed by long ones. This effect significantly impacts latency-sensitive workloads and motivates length-aware scheduling.

At each scheduling tick, the system selects a subset of pending requests whose combined prompt lengths fit within a token budget. Decoupling prefill from decode enables phase-specific scheduling, allowing us to optimize directly for TTFT.

The prompt of each request is known. Hence, we introduce a greedy Shortest Prompt First (SPF) heuristic that ranks requests by an age-adjusted score:

$$\text{score}(r_i) = l_i - \gamma \cdot (t - a_i), \quad (10)$$

where l_i is the prompt length, a_i is arrival time, t is the current time, and γ controls the anti-starvation trade-off between responsiveness (low γ) and fairness (high γ).

Requests are sorted by score and added greedily until the cumulative token limit is reached. This favors short prompts while gradually promoting delayed long requests, achieving a practical balance between latency and fairness. The full procedure is shown in Algorithm 2.

While SPF is simple in design, its deployment is facilitated by our system’s phase isolation: in monolithic schedulers, prefill prioritization is harder to isolate and tune due to shared queues and coupled resource contention. In §6.5, we show that SPF significantly reduces TTFT compared to

FCFS and helps offset performance regressions when SMs are reallocated to decode under memory pressure.

4.3.2 Decode Scheduler. The decode phase controls TBT. Unlike prefill, decode scheduling operates at a finer granularity, with each request contributing only a single token to the active batch. Thus, we adopt a simple First-Come-First-Serve (FCFS) policy. FCFS ensures fairness, incurs minimal overhead, and avoids token-level starvation. While more sophisticated schemes that consider context window size or memory bandwidth are theoretically possible, we find that their impact is limited.

5 Implementation

We implement Nexus on top of vLLM v1-0.8.1 [55], modifying approximately 6K lines of Python and CUDA/C++ code. Our changes enable phase-separated execution within a single engine or a single GPU, with minimal disruption to the original engine architecture. The maximum batch size and chunk size for prefill of Nexus are same as those of vLLM..

Concurrent Execution. We launch prefill and decode phases as separate coroutines, each managing its own GPU stream and scheduler. The main loop coordinates their execution and handles shared metadata updates. Because both phases share worker threads, we guard critical state to prevent inconsistencies during overlapping execution.

Per-Phase Scheduler. We extend vLLM’s unified scheduler with pluggable logic for phase-specific algorithms. Prefill and decode queues are maintained independently. Both schedulers are configured to use the vLLM’s default config. The SPT implementation has the default γ set to 15.

SM Partitioning and Runtime Switching. We use CUDA Green Context [35] to partition the SM. Since CUDA Green Context does not provide a Python API, we implement a PyTorch extension using approximately 150 lines of CUDA code to expose this functionality to Python. We leverage this extension to dynamically reassign SM groups at runtime. To avoid reconfiguration overhead, Nexus pre-instantiates all partition layouts during initialization and switches among them as decided by the algorithm. The decaying λ for each operator in cost model (§4.1) is obtained by profiling prefill and decode offline, and is done for each model and workload configuration. Since SPT scheduler heavily optimizes TTFT, we have a tight 1.1 β slack for decode, and 1.3 α slack for prefill. The KV_{switch} threshold is set to be 70% of all available KV cache memory.

6 Evaluation

In this section, we first examine the end-to-end performance of Nexus under various workloads. Then, we evaluate the design choices of Nexus and show the effectiveness of each component.

Dataset		Mean	P50	P95	P99
Long Data Collections	In	5905	5461	9292	9817
	Out	180	159	339	454
ArXiv Summarization	In	3832	3575	6460	6894
	Out	200	181	357	443
ShareGPT	In	496	432	970	1367
	Out	97	37	383	474

Table 1. Characteristics of Workloads. Distributions of input and output lengths of various datasets from different serving scenarios.

6.1 Experimental Setup

Testbed. Our evaluations are run on a workstation with Intel Xeon Platinum 8457C CPU (45 cores), two NVIDIA-L20 GPUs with 48GB DDR6 RAM each, and 200GB of CPU memory. The GPUs use driver 570.124.04 together with CUDA 12.8. All benchmarks were executed under PyTorch-2.6.0.

Model. We use Qwen2.5–3B and LLaMA3.1–8B for single-GPU experiments, and Qwen2.5–14B for dual-GPU setups. These popular open-source LLMs span a range of KV cache sizes and compute intensities, enabling evaluation under diverse resource pressures.

Workloads. We construct three workloads to emulate real-world LLM serving, combining datasets with diverse usage patterns and token length characteristics (Table 1). Similar to prior work [25, 67], the arrival pattern of requests is generated by a Poisson process.

- **Long Data Collections** [53]: It mixes multi-turn QA and summarization, characterized by long prefill lengths and moderate decode demands. Evaluated on Qwen2.5–3B.
- **Arxiv** [6]: It uses ArXiv Summarization [6] (full paper and abstract pairs) to model long-input, short-output tasks with stable token patterns. Evaluated on Qwen2.5–3B.
- **Mixed**: It Combines 60% ShareGPT [46] (short, interactive prompts) and 40% Long Data Collections to induce token length and KV cache variability, stressing scheduling and memory. Evaluated on LLaMA3.1–8B and Qwen2.5–14B.

Metrics. We report the mean and 95th percentile of three latency metrics: TTFT, TBT, and Normalized Latency. Normalized Latency is defined as the end-to-end latency divided by the number of output tokens, reflecting per-token serving efficiency across variable-length requests. A well-optimized serving system should maintain low normalized latency under high request loads.

Baselines. We compare Nexus against four representative LLM serving engines, all configured with the same tensor parallelism, chunked prefill, and scheduling budget for fair comparison. We plan to integrate Semi-PD in a future update to provide a more complete intra-GPU PD disaggregation system comparison.

- **vLLM (v1.0.8.1)**. A throughput-optimized serving engine with FCFS scheduling, continuous batching [62], Page Attention, and chunked prefill [1].

- **FastServe (v0.0.8.1)**. Implements a multi-level feedback queue with skip-join to resolve head-of-line blocking [56]. We reimplement it atop vLLM due to lack of public code and enable CPU swap (120GB) for each device with re-computation fallback.

- **SGLang (v0.4.4.post1)**⁴. A latency-optimized engine using Radix Attention for KV reuse [66]. Supports chunked prefill, Page Attention, and FCFS scheduling.

- **vLLM-P/D (v1.0.8.5)**. An extension of vLLM with pre-fill–decode disaggregation via LMCache [7, 28, 60]. We evaluate one prefill and one decode instance on separate GPUs to model single-layer PD setups.

6.2 End-to-end Performance

We first evaluate end-to-end performance on a single GPU using three workloads with Qwen2.5-3B and Llama3-1-8B (Section 6.2.1). All systems use one L20 GPU, except Dist-vLLM, which uses two. Then, we report multi-GPU results (Section 6.2.2).

6.2.1 End-to-End Single-GPU Performance. Figure 9 reports the end-to-end single GPU performance of Nexus and all baselines across three workloads (top to bottom). Figure 9 yields three key conclusions, which we discuss in detail below.

TTFT. As shown in Figure 9 (columns 3–4), Nexus achieves the lowest or near-lowest average TTFT across all workloads. It improves TTFT by 2–20× over vLLM and up to 1.6× over SGLang through SPF scheduling and dynamic SM reallocating. The latter reallocates GPU resources at runtime to reduce prefill–decode contention, further amplifying SPF’s benefits. vLLM and SGLang suffer from head-of-line blocking under FCFS, though SGLang fares better due to its optimized runtime. FastServe reduces average TTFT via skip-join MLFQ, but hurts P95 due to deprioritizing long prompts. Compared to vLLM-P/D, which avoids contention by separating phases across GPUs, Nexus matches its TTFT in Mixed Workload and remains within 10% on Long Data Collections and Arxiv while using a single GPU.

To ensure fairness, Nexus includes a tunable anti-starvation mechanism within its prefill scheduler. Under current settings, it improves P95 TTFT by 2–3× over vanilla vLLM and narrows the gap with SGLang and vLLM-P/D in Long Data Collections and Arxiv Workloads, while maintaining consistent advantages in average latency. In Mixed Workload, Nexus shows worse tail TTFT due to high prompt length diversity, which increases batching variability and makes it harder to protect long requests without hurting throughput.

⁴For fairness, we select the same evaluation timepoint as vLLM for SGLang; the corresponding commit is 3c09548.

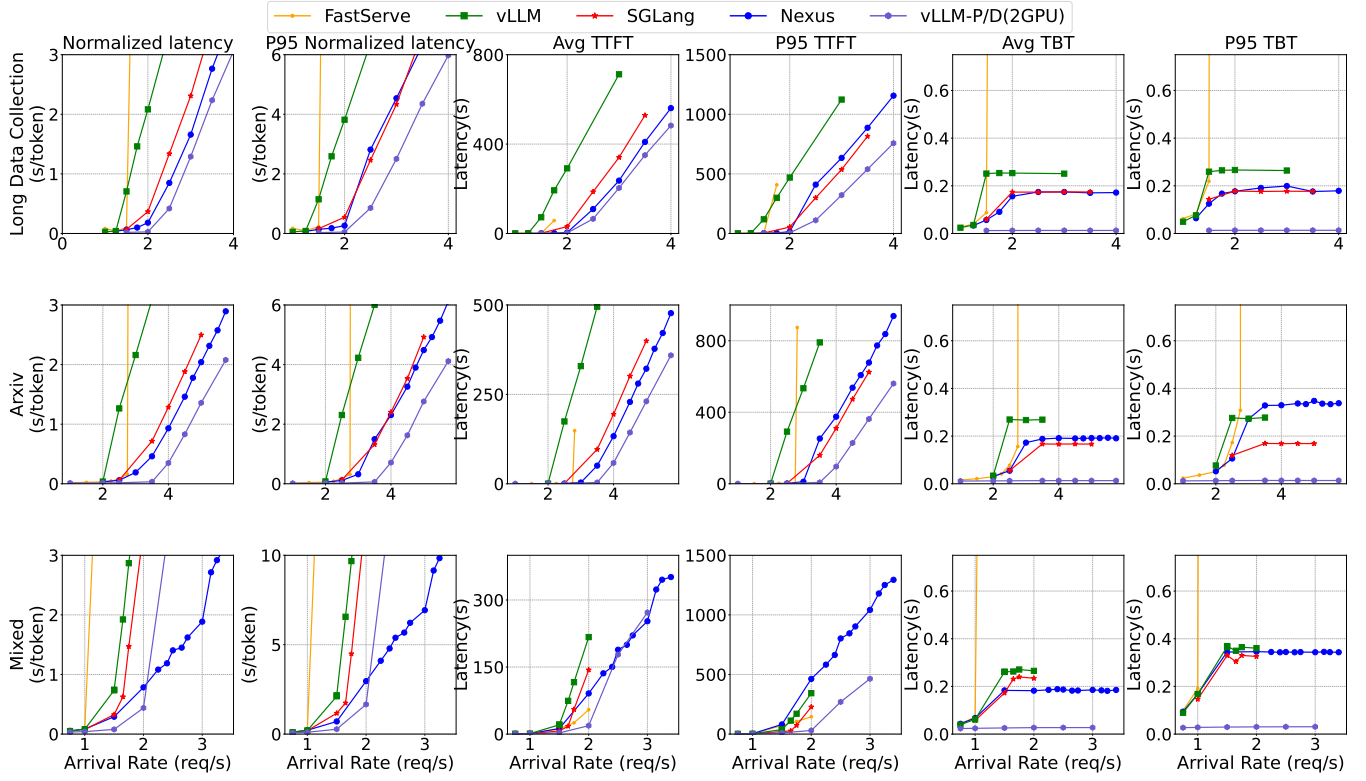


Figure 9. End-to-end results on Single GPU. All systems use a single L20 GPU, except vLLM-P/D which uses two. This figure compares three workloads: Long Data Collection and Arxiv use Qwen-2.5-3B(first two rows), and Mixed uses Llama-3-1.8B(third row). The first and second columns report the average and 95th-percentile normalized latency—lower is better for throughput. The third and fourth columns report the average and 95th-percentile TTFT, while the fifth and sixth columns show the average and 95th-percentile TBT.

TBT. TBT reflects the responsiveness of steady-state decoding, and is particularly sensitive to memory bandwidth and scheduling efficiency. As we can see from Figure 9 (columns 5–6), vLLM-P/D achieves the best average and P95 TBT by fully separating prefill and decode onto dedicated GPUs. Among single-GPU systems, Nexus consistently ranks at or near the top across all workloads.

FastServe degrades sharply under load as it needs to fall back on recomputation. vLLM, which co-schedules prefill and decode, suffers from intra-batch interference, trailing Nexus by $1.24\times$ – $1.48\times$. SGLang improves over vLLM via Radix Attention and runtime optimizations, closely matching Nexus in Long Data Collections Workload, slightly surpassing in Arxiv Workload, but falling behind in Mixed Workload where prompt diversity intensifies decode imbalance.

While Nexus lags in P95 TBT on Arxiv Workload, this anomaly stems from the workload’s relatively uniform input lengths and moderate output size (Table 1), which result in minimal memory pressure. As a consequence, the system’s dynamic SM partitioning is less likely to trigger aggressive decode resource shifts for few tailed requests.

Throughput. To summarize end-to-end performance, we also measure maximum sustainable throughput as the highest arrival rate that each system can handle without violating token latency constraints.

From Figure 9 (columns 1–2), Nexus consistently delivers the highest throughput among single-GPU systems. In Long Data Collections and Arxiv Workloads, it achieves 1.5 – $1.8\times$ higher throughput than vLLM and 1.18 – $1.27\times$ higher than SGLang, reflecting more efficient resource scheduling under uniform or moderately variable request patterns.

In Mixed Workload, where prompt diversity and scheduling imbalance are most pronounced, Nexus demonstrates its largest gain: it achieves $1.9\times$ higher throughput than vLLM, $1.8\times$ over SGLang, and even $1.4\times$ over vLLM-P/D, despite the latter using two GPUs and full-phase disaggregation. This is driven by Nexus’s head-light design which aggressively prioritizing short requests and adapting GPU resource allocation dynamically, enabling it to avoid contention and return early outputs with minimal delay.

By serving more requests under the same compute budget, Nexus not only improves user-perceived latency but also scales to higher load than other systems, evidencing its strength in practical high-throughput serving scenarios.

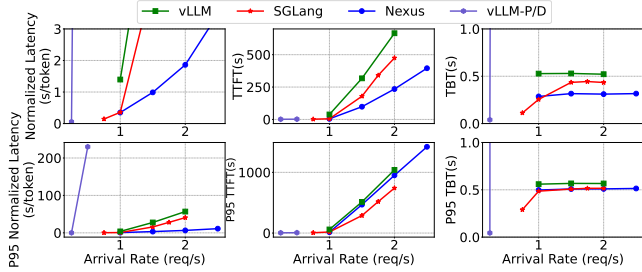


Figure 10. End-to-end results for Multi-GPU. Run using Mixed Workload on two NVIDIA L20 GPUs with Qwen2.5-14B. All systems use two L20 GPU. The top row presents average normalized latency, TTFT, and TBT, while the bottom row shows corresponding P95 metrics.

6.2.2 End-to-End Multi-GPU Performance. Due to space limits, we present multi-GPU results for Qwen-2.5-14B on the Mixed Workload only, as trends on other ones are similar. Since FastServe already performs poorly in single-GPU tests, we exclude it here and compare against stronger baselines: vLLM, SGLang, and vLLM-P/D.

As shown in Figure 10, Nexus achieves the highest throughput, $2.2\times$ over vLLM and $2\times$ over SGLang, while using the same hardware. These gains come from efficient intra-engine phase separation and the ability to maintain high concurrency without overwhelming shared compute or memory resources.

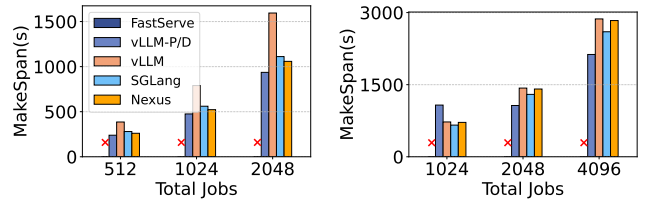
More importantly, this throughput does not come at the cost of latency. Nexus delivers $2\text{--}3\times$ lower average TTFT and $1.5\text{--}2\times$ lower TBT than vLLM and SGLang, showing strong responsiveness across both prefill and decode phases. At the tail, P95 TTFT is slightly higher than SGLang but matches vLLM, while P95 TBT is nearly identical across all systems.

One surprising result is the poor performance of vLLM-P/D despite its disaggregated architecture. Its aggressive prefill overwhelms the decode stage and saturates the transfer buffer, leading to frequent cache evictions and recomputation. Nexus, by contrast, avoids these issues through adaptive SM partitioning which dynamically changes load to sustain decoding throughput even under pressure.

In sum, Nexus offers the best latency–throughput tradeoff among all baselines, scaling to larger models while preserving per-token responsiveness and avoiding the coordination pitfalls of more fragmented systems.

6.3 Offline Inference under Heterogeneous Prompts

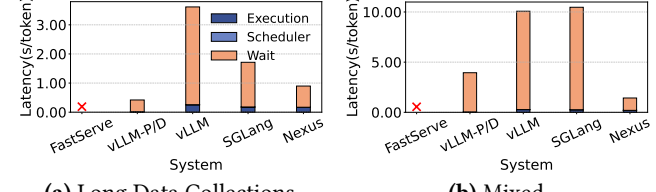
In offline settings where requests are handled in large batches, throughput should be prioritized over latency. To evaluate this scenario, we submit all requests at once and measure end-to-end makespan. As shown in Figure 11, Nexus achieves 5–50% lower makespan than vLLM and SGLang on Long Data Collections, which features uniformly long requests that benefit from phase separation and adaptive GPU resource use. In Mixed Workload, with highly variable input lengths, Nexus



(a) Long Data Collections.

(b) Mixed.

Figure 11. Offline Inference. Run on a single L20 under Long Data Collections and Mixed Workloads with 3B and 8B models respectively. X means timeout. All systems use a single L20 GPU, except vLLM-P/D with two.



(a) Long Data Collections.

(b) Mixed.

Figure 12. Breakdown of Inference Overheads. Run on a single L20 under Long Data Collections and Mixed Workloads with 3B and 8B models respectively. X means timeout. All systems use a single L20 GPU, except vLLM-P/D with a single L20 GPU.

still outperforms vLLM by 5% but lags SGLang by 8–15% due to its stronger tail control. FastServe times out under both workloads. vLLM-P/D achieves 15%–35% lower makespan than Nexus but needs more GPU.

6.4 Latency Breakdown

To better understand the sources of Nexus’s performance gains, Figure 12 decomposes normalized token latency into scheduling, queuing, and execution stages.

Scheduling Overhead. All systems incur minimal scheduling latency. Nexus’s dual-queue design introduces no measurable overhead, confirming its coordination logic is lightweight.

Execution Time. Execution latency under Nexus closely matches that of vLLM and SGLang. Although Nexus runs prefill and decode in separate batches, which leads to reading model weights more than once, its batch level separation and dynamic resource use help reduce contention, keeping the overhead low. vLLM-P/D achieves the lowest execution latency due to full disaggregation, but at the cost of using twice GPUs.

Queuing Delay. Waiting time dominates total latency under load, and here Nexus demonstrates its greatest advantage. In Long Data Collections, Nexus reduces waiting time by $4\times$ over vLLM and $2\times$ over SGLang. In Mixed Workload, which involves greater request variability, it improves further, achieving $5\times$ lower wait time than monolithic baselines, and $2\times$ less than vLLM-P/D. These gains stem from

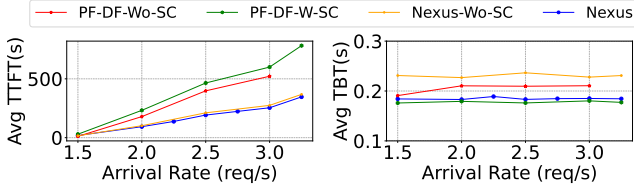


Figure 13. Ablation Study. Run with Mixed Workload on Llama3.1-8B using a single L20 GPU. *PF-DF-Wo-SC* is the intra-engine PD disaggregation that uses FCFS for both prefill and decode scheduling, without dynamical GPU SM changing. *PF-DF-W-SC* is the intra-engine PD disaggregation that FCFS scheduling for both prefill and decode but enables dynamical GPU SM changing. *Nexus-Wo-SC* denotes our system with dynamical GPU SM changing disabled.

Nexus’s effective shortest-prompt-first scheduling and adaptive GPU resource allocation, allowing it to maintain concurrency without overloading shared resources.

6.5 Ablation Study

We ablate Nexus’s two core components: (1) dynamic SM changing and (2) phase-specific scheduling, with focus on Shortest-Prompt-First (SPF) for prefill. Figure 13 shows the results.

Baseline: FCFS Scheduling(Naive Intra-Engine PD Disaggregation). The baseline (PF-DF-Wo-SC) is the intra-engine PD disaggregation that uses FCFS for both prefill and decode without dynamic SM changing. It suffers from head-of-line (HOL) blocking in prefill and persistent resource contention between phases, resulting in poor TTFT and TBT.

Effect of Dynamical SM Changing. Enabling dynamic SM changing (PF-DF-W-SC) improves TBT by 14% over the baseline by assigning more compute to decode when GPU memory becomes bottleneck. However, TTFT degrades by 30% due to delayed prefill execution during decode intervals. This showcases the inevitable TBT and TTFT tradeoff under naive FCFS.

Effect of Prefill Scheduling (SPF without SM Changing). Applying SPF to prefill (Nexus-Wo-SC) dramatically improves TTFT (up to 90% reduction over baseline) by mitigating HOL blocking. However, TBT worsens, due to unresolved GPU resource contention between prefill and decode. SPF helps responsiveness, but lacks decode-phase control.

Combined Design: SPF + Dynamical SM Changing When both techniques are used (Nexus), TTFT improves by 23% over SPF-only, while TBT drops by 26%, achieving optimality. Unlike FCFS+switching, TTFT does not regress, as SPF reduces prefill HOL blocking and can benefit from less contention. Dynamical SM changing amplifies gains without introducing new overhead.

7 Related Work

Monolithic LLM Serving Systems. Early LLM serving engines focus on maximizing throughput and memory efficiency within a unified execution engine. Orca [62] introduces continuous batching to reduce head-of-line blocking. vLLM [25] eliminates KV cache fragmentation via PagedAttention, while SGLang [66] reduces memory usage through RadixAttention. SarathiServe [1] mixes chunks of prefill and decode requests to better utilize GPU resources. However, all of these designs treat prefill and decode as indistinguishable units within a shared queue. In contrast, **Nexus** decouples the two phases at the batching level, enabling independent, phase-specific execution and scheduling while preserving compatibility with existing attention mechanisms.

Engine-Level PD Disaggregation Systems. Several systems physically disaggregate prefill and decode across GPUs to better match their resource profiles. Splitwise [42] statically assigns phases to different hardware tiers; DistServe [67] improves TTFT/TBT via tiered GPU scheduling; Mooncake [45] serves cached KV blocks from storage to reduce compute load; TetriInfer [23] routes requests by latency class to isolated replicas. **Nexus** achieves similar benefits without incurring cross-engine complexity. By performing lightweight intra-engine disaggregation, it enables low-latency execution and efficient KV reuse within a single serving engine.

Intra-GPU PD Disaggregation Systems. Recent systems like Bullet [26], Drift [9], and semi-PD [22] explore intra-GPU disaggregation to reduce cross-device overhead. Bullet builds profile-augmented latency models and uses SLO-driven feedback loops to tune SM partitioning reactively. Drift applies phase-tagged gang scheduling under a contention-free assumption, combining static modeling with latency-aware dispatch. Semi-PD fits inverse-linear latency curves and adjusts SM ratios through runtime feedback control based on latency violations. **Nexus** takes a proactive approach. First, it introduces a contention-aware analytical model that explicitly captures both diminishing compute returns and dynamic memory bandwidth interference at the operator level. Second, it formulates intra-GPU resource allocation as a dual-objective optimization problem guided by runtime KV-cache usage and solved via fast greedy search. Third, Nexus uses a one-time profiling pass to calibrate per-kernel latency scaling curves, but avoids offline workload tracing or in-deployment feedback fitting, enabling generalization across dynamic traffic and prompt structures.

GPU Multiplexing. Work on GPU multiplexing explores spatial or temporal sharing across models or processes. Systems like GPUlet, Orion, REEF, and Bless [8, 21, 49, 65] optimize for small models via fine-grained temporal sharing. MuxServe [13] proposes spatial-temporal multiplexing to efficiently serve multiple LLMs, while NanoFlow [68] and Liger [12] introduce kernel level parallelism that enables concurrent execution of compute bound, network bound,

and memory bound operations. Unlike these systems, which focus on generic sharing or inter-model concurrency, **Nexus** targets intra-GPU, phase-level disaggregation. It dynamically and proactively reallocates GPU resources between prefill and decode phases within a single LLM engine, enabling fine-grained, workload-aware partitioning guided by lightweight performance modeling and coordinated scheduling.

LLM Scheduling Frameworks. Prior works also propose sophisticated schedulers to balance latency and throughput. FastServe [56] uses MLFQ with skip-join to avoid prompt variance stalls. VTC [47] and QLM [43] target fairness and SLO adherence. Llumnix [50] accelerates dynamic scaling via migration-aware scheduling. LightLLM [17] and Preble [48] improve memory reuse via future prediction or prompt sharing. Yet, all treat each request as a monolithic scheduling unit. **Nexus** introduces dual schedulers for prefill and decode, each tailored to its phase’s latency sensitivity and compute intensity. This decoupling enables tighter queue control and more efficient GPU resource utilization.

8 Conclusion

While the asymmetric demands of prefill and decode in LLM inference are well known, their combined impact on intra-GPU contention under dynamic workloads remains underexplored. We show that static isolation and reactive control fall short in managing compute saturation, memory and memory bandwidth contention. Nexus addresses this via a lightweight analytical model, dual-objective optimization, and phase-specific schedulers for proactive, sub-second resource reallocation. Across diverse models and workloads, Nexus improves both throughput and latency, outperforming monolithic and disaggregated baselines with fewer resources.

9 Acknowledgement

We sincerely thank Zikun Li, Xinhao Cheng, Mingyu Li, Linsong Guo, Lisan Wu, Xupeng Miao, Shulai Zhang, Zihao Ye, Xiyuan Cui, Zhanda Zhu, Zhihao Jia, Xingda Wei and Yubin Xia for their kind help on this paper.

References

[1] Amey Agrawal, Nitin Kedia, Ashish Panwar, Jayashree Mohan, Nipun Kwatra, Bhargav S. Gulavani, Alexey Tumanov, and Ramachandran Ramjee. 2024. Taming Throughput-Latency Tradeoff in LLM Inference with Sarathi-Serve. In *18th USENIX Symposium on Operating Systems Design and Implementation, OSDI 2024, Santa Clara, CA, USA, July 10-12, 2024*, Ada Gavrilovska and Douglas B. Terry (Eds.). USENIX Association, 117–134. <https://www.usenix.org/conference/osdi24/presentation/agrawal>

[2] Jinze Bai, Shuai Bai, Yunfei Chu, Zeyu Cui, Kai Dang, Xiaodong Deng, Yang Fan, Wenbin Ge, Yu Han, Fei Huang, et al. 2023. Qwen technical report. *arXiv preprint arXiv:2309.16609* (2023).

[3] Jinze Bai, Shuai Bai, Yunfei Chu, Zeyu Cui, Kai Dang, Xiaodong Deng, Yang Fan, Wenbin Ge, Yu Han, Fei Huang, Binyuan Hui, Luo Ji, Mei Li, Junyang Lin, Runji Lin, Dayiheng Liu, Gao Liu, Chengqiang Lu, Keming Lu, Jianxin Ma, Rui Men, Xingzhang Ren, Xuancheng Ren, Chuanqi Tan, Sinan Tan, Jianhong Tu, Peng Wang, Shijie Wang, Wei Wang, Shengguang Wu, Benfeng Xu, Jin Xu, An Yang, Hao Yang, Jian Yang, Shusheng Yang, Yang Yao, Bowen Yu, Hongyi Yuan, Zheng Yuan, Jianwei Zhang, Xingxuan Zhang, Yichang Zhang, Zhenru Zhang, Chang Zhou, Jingren Zhou, Xiaohuan Zhou, and Tianhang Zhu. 2023. Qwen Technical Report. *arXiv:2309.16609 [cs.CL]* <https://arxiv.org/abs/2309.16609>

[4] Tom B. Brown, Benjamin Mann, Nick Ryder, Melanie Subbiah, Jared Kaplan, Prafulla Dhariwal, Arvind Neelakantan, Pranav Shyam, Girish Sastry, Amanda Askell, Sandhini Agarwal, Ariel Herbert-Voss, Gretchen Krueger, Tom Henighan, Rewon Child, Aditya Ramesh, Daniel M. Ziegler, Jeffrey Wu, Clemens Winter, Christopher Hesse, Mark Chen, Eric Sigler, Mateusz Litwin, Scott Gray, Benjamin Chess, Jack Clark, Christopher Berner, Sam McCandlish, Alec Radford, Ilya Sutskever, and Dario Amodei. 2020. Language Models are Few-Shot Learners. In *Advances in Neural Information Processing Systems 33: Annual Conference on Neural Information Processing Systems 2020, NeurIPS 2020, December 6-12, 2020, virtual*, Hugo Larochelle, Marc’Aurelio Ranzato, Raia Hadsell, Maria-Florina Balcan, and Hsuan-Tien Lin (Eds.). <https://proceedings.neurips.cc/paper/2020/hash/1457c0d6bfcba4967418bf8ac142f64a-Abstract.html>

[5] Tom B. Brown, Benjamin Mann, Nick Ryder, Melanie Subbiah, Jared Kaplan, Prafulla Dhariwal, Arvind Neelakantan, Pranav Shyam, Girish Sastry, Amanda Askell, Sandhini Agarwal, Ariel Herbert-Voss, Gretchen Krueger, Tom Henighan, Rewon Child, Aditya Ramesh, Daniel M. Ziegler, Jeffrey Wu, Clemens Winter, Christopher Hesse, Mark Chen, Eric Sigler, Mateusz Litwin, Scott Gray, Benjamin Chess, Jack Clark, Christopher Berner, Sam McCandlish, Alec Radford, Ilya Sutskever, and Dario Amodei. 2020. Language Models are Few-Shot Learners. *arXiv:2005.14165 [cs.CL]* <https://arxiv.org/abs/2005.14165>

[6] ccdv. 2025. arxiv-summarization. <https://huggingface.co/datasets/ccdv/arxiv-summarization>.

[7] Yihua Cheng, Kuntai Du, Jiayi Yao, and Junchen Jiang. 2024. Do Large Language Models Need a Content Delivery Network? *arXiv preprint arXiv:2409.13761* (2024).

[8] Seungbeom Choi, Sunho Lee, Yeonjae Kim, Jongse Park, Youngjin Kwon, and Jaehyuk Huh. 2022. Serving Heterogeneous Machine Learning Models on Multi-GPU Servers with Spatio-Temporal Sharing. In *Proceedings of the 2022 USENIX Annual Technical Conference, USENIX ATC 2022, Carlsbad, CA, USA, July 11-13, 2022*, Jiri Schindler and Noa Zilberman (Eds.). USENIX Association, 199–216. <https://www.usenix.org/conference/atc22/presentation/choi-seungbeom>

[9] Weihao Cui, Yukang Chen, Han Zhao, Ziyi Xu, Quan Chen, Xusheng Chen, Yangjie Zhou, Shixuan Sun, and Minyi Guo. 2025. Optimizing SLO-oriented LLM Serving with PD-Multiplexing. *CoRR abs/2504.14489* (2025). <https://doi.org/10.48550/ARXIV.2504.14489> *arXiv:2504.14489*

[10] Cursor. 2025. Cursor. <https://www.cursor.com/>.

[11] DeepSeek. 2025. DeepSeek. <https://www.deepseek.com/>.

[12] Jiangsu Du, Jinhui Wei, Jiazhij Jiang, Shenggan Cheng, Dan Huang, Zhiguang Chen, and Yutong Lu. 2024. Liger: Interleaving Intra- and Inter-Operator Parallelism for Distributed Large Model Inference. In *Proceedings of the 29th ACM SIGPLAN Annual Symposium on Principles and Practice of Parallel Programming, PPoPP 2024, Edinburgh, United Kingdom, March 2-6, 2024*, Michel Steuwer, I-Ting Angelina Lee, and Milind Chabbi (Eds.). ACM, 42–54. <https://doi.org/10.1145/3627535.3638466>

[13] Jiangfei Duan, Runyu Lu, Haojie Duanmu, XiuHong Li, Xingcheng Zhang, Dahua Lin, Ion Stoica, and Hao Zhang. 2024. MuxServe: Flexible Spatial-Temporal Multiplexing for Multiple LLM Serving. In *Forty-first International Conference on Machine Learning, ICML 2024, Vienna, Austria, July 21-27, 2024*. OpenReview.net. <https://openreview.net/forum?id=R0SoZvqXyQ>

[14] Abhimanyu Dubey, Abhinav Jauhri, Abhinav Pandey, Abhishek Kadian, Ahmad Al-Dahle, Aiesha Letman, Akhil Mathur, Alan Schellen, Amy Yang, Angela Fan, Anirudh Goyal, Anthony Hartshorn, Aobo Yang, Archi Mitra, Archie Sravankumar, Artem Korenev, Arthur Hinsvark, Arun Rao, Aston Zhang, Aurélien Rodriguez, Austen Greggerson, Ava Spataru, Baptiste Rozière, Bethany Biron, Binh Tang, Bobbie Chern, Charlotte Caucheteux, Chaya Nayak, Chloe Bi, Chris Marra, Chris McConnell, Christian Keller, Christophe Touret, Chongyang Wu, Corinne Wong, Cristian Canton Ferrer, Cyrus Nikolaidis, Damien Allonsius, Daniel Song, Danielle Pintz, Danny Livshits, David Esiobu, Dhruv Choudhary, Dhruv Mahajan, Diego Garcia-Olano, Diego Perino, Dieuwke Hupkes, Egor Lakomkin, Ehab AlBadawy, Elina Lobanova, Emily Dinan, Eric Michael Smith, Filip Radenovic, Frank Zhang, Gabriel Synnaeve, Gabrielle Lee, Georgia Lewis Anderson, Graeme Nail, Grégoire Mialon, Guan Pang, Guillem Cucurell, Hailey Nguyen, Hannah Korevaar, Hu Xu, Hugo Touvron, Iliyan Zarov, Imanol Arrieta Ibarra, Isabel M. Kloumann, Ishan Misra, Ivan Evtimov, Jade Copet, Jaewon Lee, Jan Geffert, Jana Vranes, Jason Park, Jay Mahadeokar, Jeet Shah, Jelmer van der Linde, Jennifer Billock, Jenny Hong, Jenya Lee, Jeremy Fu, Jianfeng Chi, Jianyu Huang, Jiawen Liu, Jie Wang, Jiecao Yu, Joanna Bitton, Joe Spisak, Jongsoo Park, Joseph Rocca, Joshua Johnstun, Joshua Saxe, Junteng Jia, Kalyan Vasudevan Alwala, Kartikeya Upasani, Kate Plawiak, Ke Li, Kenneth Heafield, Kevin Stone, and et al. 2024. The Llama 3 Herd of Models. *CoRR* abs/2407.21783 (2024). <https://doi.org/10.48550/ARXIV.2407.21783>

[15] Jingqi Feng, Yukai Huang, Rui Zhang, Sicheng Liang, Ming Yan, and Jie Wu. 2025. WindServe: Efficient Phase-Disaggregated LLM Serving with Stream-based Dynamic Scheduling. In *Proceedings of the 52nd Annual International Symposium on Computer Architecture*. 1283–1295.

[16] GigaSpaces. 2023. *Amazon Found Every 100ms of Latency Cost them 1% in Sales*. <https://www.gigaspaces.com/blog/amazon-found-every-100ms-of-latency-cost-them-1-in-sales> Accessed: 2025-05-28.

[17] Ruihao Gong, Shihao Bai, Siyu Wu, Yunqian Fan, Zaijun Wang, Xiuhong Li, Hailong Yang, and Xianglong Liu. 2025. Past-Future Scheduler for LLM Serving under SLA Guarantees. In *Proceedings of the 30th ACM International Conference on Architectural Support for Programming Languages and Operating Systems, Volume 2, ASPLOS 2025, Rotterdam, Netherlands, 30 March 2025 - 3 April 2025*, Lieven Eeckhout, Georgios Smaragdakis, Katai Liang, Adrian Sampson, Martha A. Kim, and Christopher J. Rossbach (Eds.). ACM, 798–813. <https://doi.org/10.1145/3676641.3716011>

[18] Google. 2025. gemini. <https://gemini.google.com/>.

[19] Daya Guo, Dejian Yang, Haowei Zhang, Junxiao Song, Ruoyu Zhang, Runxin Xu, Qihao Zhu, Shirong Ma, Peiyi Wang, Xiao Bi, et al. 2025. Deepseek-r1: Incentivizing reasoning capability in llms via reinforcement learning. *arXiv preprint arXiv:2501.12948* (2025).

[20] Daya Guo, Qihao Zhu, Dejian Yang, Zhenda Xie, Kai Dong, Wentao Zhang, Guanting Chen, Xiao Bi, Yu Wu, YK Li, et al. 2024. DeepSeek-Coder: When the Large Language Model Meets Programming—The Rise of Code Intelligence. *arXiv preprint arXiv:2401.14196* (2024).

[21] Mingcong Han, Hanze Zhang, Rong Chen, and Haibo Chen. 2022. Microsecond-scale Preemption for Concurrent GPU-accelerated DNN Inferences. In *16th USENIX Symposium on Operating Systems Design and Implementation, OSDI 2022, Carlsbad, CA, USA, July 11-13, 2022*, Marcos K. Aguilera and Hakim Weatherspoon (Eds.). USENIX Association, 539–558. <https://www.usenix.org/conference/osdi22/presentation/han>

[22] Ke Hong, Lufang Chen, Zhong Wang, Xiuhong Li, Qiuli Mao, Jianping Ma, Chao Xiong, Guanyu Wu, Buhe Han, Guohao Dai, Yun Liang, and Yu Wang. 2025. semi-PD: Towards Efficient LLM Serving via Phase-Wise Disaggregated Computation and Unified Storage. [arXiv:2504.19867 \[cs.CL\]](https://arxiv.org/abs/2504.19867) <https://arxiv.org/abs/2504.19867>

[23] Cunchen Hu, Heyang Huang, Liangliang Xu, Xusheng Chen, Jiang Xu, Shuang Chen, Hao Feng, Chenxi Wang, Sa Wang, Yungang Bao, Ninghui Sun, and Yizhou Shan. 2024. Inference without Interference: Disaggregate LLM Inference for Mixed Downstream Workloads. *CoRR* abs/2401.11181 (2024). <https://doi.org/10.48550/ARXIV.2401.11181> arXiv:2401.11181

[24] Aditya K. Kamath, Ramya Prabhu, Jayashree Mohan, Simon Peter, Ramachandran Ramjee, and Ashish Panwar. 2025. POD-Attention: Unlocking Full Prefill-Decode Overlap for Faster LLM Inference. In *Proceedings of the 30th ACM International Conference on Architectural Support for Programming Languages and Operating Systems, Volume 2, ASPLOS 2025, Rotterdam, Netherlands, 30 March 2025 - 3 April 2025*, Lieven Eeckhout, Georgios Smaragdakis, Katai Liang, Adrian Sampson, Martha A. Kim, and Christopher J. Rossbach (Eds.). ACM, 897–912. <https://doi.org/10.1145/3676641.3715996>

[25] Woosuk Kwon, Zhuohan Li, Siyuan Zhuang, Ying Sheng, Lianmin Zheng, Cody Hao Yu, Joseph Gonzalez, Hao Zhang, and Ion Stoica. 2023. Efficient Memory Management for Large Language Model Serving with PagedAttention. In *Proceedings of the 29th Symposium on Operating Systems Principles, SOSP 2023, Koblenz, Germany, October 23-26, 2023*, Jason Flinn, Margo I. Seltzer, Peter Druschel, Antoine Kaufmann, and Jonathan Mace (Eds.). ACM, 611–626. <https://doi.org/10.1145/3600006.3613165>

[26] Zejia Lin, Hongxin Xu, Guanyi Chen, Xianwei Zhang, and Yutong Lu. 2025. Bullet: Boosting GPU Utilization for LLM Serving via Dynamic Spatial-Temporal Orchestration. [arXiv:2504.19516 \[cs.DC\]](https://arxiv.org/abs/2504.19516) <https://arxiv.org/abs/2504.19516>

[27] Aixin Liu, Bei Feng, Bing Xue, Bingxuan Wang, Bochao Wu, Chengda Lu, Chenggang Zhao, Chengqi Deng, Chenyu Zhang, Chong Ruan, et al. 2024. Deepseek-v3 technical report. *arXiv preprint arXiv:2412.19437* (2024).

[28] Yuhang Liu, Hanchen Li, Yihua Cheng, Siddhant Ray, Yuyang Huang, Qizheng Zhang, Kuntai Du, Jiayi Yao, Shan Lu, Ganesh Ananthanarayanan, et al. 2024. Cachegen: Kv cache compression and streaming for fast large language model serving. In *Proceedings of the ACM SIGCOMM 2024 Conference*. 38–56.

[29] Michael Luo, Sijun Tan, Roy Huang, Ameen Patel, Alpay Ariyak, Qingyang Wu, Xiaoxiang Shi, Rachel Xin, Colin Cai, Maurice Weber, et al. 2025. Deepcoder: A fully open-source 14b coder at o3-mini level. *Notion Blog* (2025).

[30] Yixuan Mei, Yonghao Zhuang, Xupeng Miao, Juncheng Yang, Zhihao Jia, and Rashmi Vinayak. 2025. Helix: Serving large language models over heterogeneous gpus and network via max-flow. In *Proceedings of the 30th ACM International Conference on Architectural Support for Programming Languages and Operating Systems, Volume 1*. 586–602.

[31] Xupeng Miao, Gabriele Oliaro, Zhihao Zhang, Xinhao Cheng, Zeyu Wang, Zhengxin Zhang, Rae Ying Yee Wong, Alan Zhu, Lijie Yang, Xiaoxiang Shi, et al. 2024. Specinfer: Accelerating large language model serving with tree-based speculative inference and verification. In *Proceedings of the 29th ACM International Conference on Architectural Support for Programming Languages and Operating Systems, Volume 3*. 932–949.

[32] Xupeng Miao, Chunran Shi, Jiangfei Duan, Xiaoli Xi, Dahu Lin, Bin Cui, and Zhihao Jia. 2024. Spotserve: Serving generative large language models on preemptible instances. In *Proceedings of the 29th ACM International Conference on Architectural Support for Programming Languages and Operating Systems, Volume 2*. 1112–1127.

[33] Nvidia. 2024. FasterTransformer. <https://github.com/NVIDIA/FasterTransformer>.

[34] Nvidia. 2025. B200. <https://resources.nvidia.com/en-us-blackwell-architecture>.

[35] Nvidia. 2025. CUDA Driver API: Green COntexts. https://docs.nvidia.com/cuda/cuda-driver-api/group__CUDA__GREEN__CO CONTEXTS.html.

[36] Nvidia. 2025. H100. <https://resources.nvidia.com/en-us-hopper-architecture/nvidia-h100-tensor-c>.

[37] Nvidia. 2025. MIG. [https://www.nvidia.com/en-sg/technologies/multi-instance-gpu/..](https://www.nvidia.com/en-sg/technologies/multi-instance-gpu/).

[38] Nvidia. 2025. MPS. <https://docs.nvidia.com/deploy/mps/contents.html>.

[39] Hyungjun Oh, Kihong Kim, Jaemin Kim, Sungkyun Kim, Junyeol Lee, Du-Seong Chang, and Jiwon Seo. 2024. ExeGPT: Constraint-Aware Resource Scheduling for LLM Inference. In *Proceedings of the 29th ACM International Conference on Architectural Support for Programming Languages and Operating Systems, Volume 2, ASPLOS 2024, La Jolla, CA, USA, 27 April 2024- 1 May 2024, Rajiv Gupta, Nael B. Abu-Ghazaleh, Madan Musuvathi, and Dan Tsafrir (Eds.)*. ACM, 369–384. <https://doi.org/10.1145/3620665.3640383>

[40] OpenAI. 2023. GPT-4 Technical Report. *CoRR* abs/2303.08774 (2023). <https://doi.org/10.48550/ARXIV.2303.08774> arXiv:2303.08774

[41] OpenAI. 2025. ChatGPT. <https://chatgpt.com>.

[42] Pratyush Patel, Esha Choukse, Chaojie Zhang, Aashaka Shah, Íñigo Goiri, Saeed Maleki, and Ricardo Bianchini. 2024. Splitwise: Efficient Generative LLM Inference Using Phase Splitting. In *51st ACM/IEEE Annual International Symposium on Computer Architecture, ISCA 2024, Buenos Aires, Argentina, June 29 - July 3, 2024*. IEEE, 118–132. <https://doi.org/10.1109/ISCA59077.2024.00019>

[43] Archit Patke, Dhemath Reddy, Saurabh Jha, Haoran Qiu, Christian Pinto, Chandra Narayanaswami, Zbigniew Kalbarczyk, and Ravishankar K. Iyer. 2024. Queue Management for SLO-Oriented Large Language Model Serving. In *Proceedings of the 2024 ACM Symposium on Cloud Computing, SoCC 2024, Redmond, WA, USA, November 20-22, 2024*. ACM, 18–35. <https://doi.org/10.1145/3698038.3698523>

[44] perplexity. 2025. perplexity. <https://www.perplexity.ai/>.

[45] Ruoyu Qin, Zheming Li, Weiran He, Jialei Cui, Feng Ren, Mingxing Zhang, Yongwei Wu, Weimin Zheng, and Xinran Xu. 2025. Mooncake: Trading More Storage for Less Computation — A KVCache-centric Architecture for Serving LLM Chatbot. In *23rd USENIX Conference on File and Storage Technologies (FAST 25)*. USENIX Association, Santa Clara, CA, 155–170. <https://www.usenix.org/conference/fast25/presentation/qin>

[46] ShareGPT. 2025. ShareGPT. https://huggingface.co/datasets/anon8231489123/ShareGPT_Vicuna_unfiltered/resolve/main/ShareGPT_V3_unfiltered_cleaned_split.json.

[47] Ying Sheng, Shiyi Cao, Dacheng Li, Banghua Zhu, Zhuohan Li, Danyang Zhuo, Joseph E. Gonzalez, and Ion Stoica. 2024. Fairness in Serving Large Language Models. In *18th USENIX Symposium on Operating Systems Design and Implementation, OSDI 2024, Santa Clara, CA, USA, July 10-12, 2024*. Ada Gavrilovska and Douglas B. Terry (Eds.). USENIX Association, 965–988. <https://www.usenix.org/conference/osdi24/presentation/sheng>

[48] Vikranth Srivatsa, Zijian He, Reyna Abhyankar, Dongming Li, and Yiyi Zhang. 2024. Preble: Efficient Distributed Prompt Scheduling for LLM Serving. *CoRR* abs/2407.00023 (2024). <https://doi.org/10.48550/ARXIV.2407.00023> arXiv:2407.00023

[49] Foteini Strati, Xianzhe Ma, and Ana Klimovic. 2024. Orion: Interference-aware, Fine-grained GPU Sharing for ML Applications. In *Proceedings of the Nineteenth European Conference on Computer Systems, EuroSys 2024, Athens, Greece, April 22-25, 2024*. ACM, 1075–1092. <https://doi.org/10.1145/3627703.3629578>

[50] Biao Sun, Ziming Huang, Hanyu Zhao, Wencong Xiao, Xinyi Zhang, Yong Li, and Wei Lin. 2024. Llumnix: Dynamic Scheduling for Large Language Model Serving. In *18th USENIX Symposium on Operating Systems Design and Implementation, OSDI 2024, Santa Clara, CA, USA, July 10-12, 2024*. Ada Gavrilovska and Douglas B. Terry (Eds.). USENIX Association, 173–191. <https://www.usenix.org/conference/osdi24/presentation/sun-biao>

[51] Kimi Team, Angang Du, Bofei Gao, Bowei Xing, Changjiu Jiang, Cheng Chen, Cheng Li, Chenjun Xiao, Chenzhuang Du, Chonghua Liao, et al. 2025. Kimi k1. 5: Scaling reinforcement learning with llms. *arXiv preprint arXiv:2501.12599* (2025).

[52] SGLang team. 2025. SGLang-v0.4. <https://lmsys.org/blog/2024-12-04-sqlang-v0-4/>.

[53] TogetherComputer. 2025. Long-Data-Collections. <https://huggingface.co/datasets/togethercomputer/Long-Data-Collections>.

[54] Ashish Vaswani, Noam Shazeer, Niki Parmar, Jakob Uszkoreit, Llion Jones, Aidan N. Gomez, Łukasz Kaiser, and Illia Polosukhin. 2017. Attention Is All You Need. *CoRR* abs/1706.03762 (2017). arXiv:1706.03762 <http://arxiv.org/abs/1706.03762>

[55] vLLM team. 2025. vLLM-v1. <https://blog.vllm.ai/2025/01/27/v1-alpha-release.html>.

[56] Bingyang Wu, Yinmin Zhong, Zili Zhang, Gang Huang, Xuanzhe Liu, and Xin Jin. 2023. Fast Distributed Inference Serving for Large Language Models. *CoRR* abs/2305.05920 (2023). <https://doi.org/10.48550/ARXIV.2305.05920> arXiv:2305.05920

[57] Jiaming Xu, Jiayi Pan, Yongkang Zhou, Siming Chen, Jinhao Li, Yaoxiu Lian, Junyi Wu, and Guohao Dai. 2025. Specee: Accelerating large language model inference with speculative early exiting. In *Proceedings of the 52nd Annual International Symposium on Computer Architecture*. 467–481.

[58] An Yang, Anfeng Li, Baosong Yang, Beichen Zhang, Binyuan Hui, Bo Zheng, Bowen Yu, Chang Gao, Chengan Huang, Chenxu Lv, et al. 2025. Qwen3 technical report. *arXiv preprint arXiv:2505.09388* (2025).

[59] An Yang, Baosong Yang, Beichen Zhang, Binyuan Hui, Bo Zheng, Bowen Yu, Chengyuan Li, Dayiheng Liu, Fei Huang, Haoran Wei, Huan Lin, Jian Yang, Jianhong Tu, Jianwei Zhang, Jianxin Yang, Jiaxi Yang, Jingren Zhou, Junyang Lin, Kai Dang, Keming Lu, Keqin Bao, Kexin Yang, Le Yu, Mei Li, Mingfeng Xue, Pei Zhang, Qin Zhu, Rui Men, Runji Lin, Tianhao Li, Tingyu Xia, Xingzhang Ren, Xuancheng Ren, Yang Fan, Yang Su, Yichang Zhang, Yu Wan, Yuqiong Liu, Zeyu Cui, Zhenru Zhang, and Zihan Qiu. 2024. Qwen2.5 Technical Report. *arXiv preprint arXiv:2412.15115* (2024).

[60] Jiayi Yao, Hanchen Li, Yuhan Liu, Siddhant Ray, Yihua Cheng, Qizheng Zhang, Kuntai Du, Shan Lu, and Junchen Jiang. 2024. CacheBlend: Fast Large Language Model Serving with Cached Knowledge Fusion. *arXiv preprint arXiv:2405.16444* (2024).

[61] Zihao Ye, Lequn Chen, Ruihang Lai, Wuwei Lin, Yineng Zhang, Stephanie Wang, Tianqi Chen, Baris Kasikci, Vinod Grover, Arvind Krishnamurthy, and Luis Ceze. 2025. FlashInfer: Efficient and Customizable Attention Engine for LLM Inference Serving. *arXiv preprint arXiv:2501.01005* (2025). <https://arxiv.org/abs/2501.01005>

[62] Gyeong-In Yu, Joo Seong Jeong, Geon-Woo Kim, Soojeong Kim, and Byung-Gon Chun. 2022. Orca: A Distributed Serving System for Transformer-Based Generative Models. In *16th USENIX Symposium on Operating Systems Design and Implementation, OSDI 2022, Carlsbad, CA, USA, July 11-13, 2022*. Marcos K. Aguilera and Hakim Weatherpoon (Eds.). USENIX Association, 521–538. <https://www.usenix.org/conference/osdi22/presentation/yu>

[63] Lingfan Yu, Jinkun Lin, and Jinyang Li. 2025. Stateful large language model serving with pensieve. In *Proceedings of the Twentieth European Conference on Computer Systems*. 144–158.

[64] Haochen Yuan, Yuanqing Wang, Wenhao Xie, Yu Cheng, Ziming Miao, Lingxiao Ma, Jilong Xue, and Zhi Yang. 2025. NeuStream: Bridging Deep Learning Serving and Stream Processing. In *Proceedings of the Twentieth European Conference on Computer Systems*. 671–685.

[65] Shulai Zhang, Quan Chen, Weihao Cui, Han Zhao, Chunyu Xue, Zhen Zheng, Wei Lin, and Minyi Guo. 2025. Improving GPU Sharing Performance through Adaptive Bubbleless Spatial-Temporal Sharing. In *Proceedings of the Twentieth European Conference on Computer Systems, EuroSys 2025, Rotterdam, The Netherlands, 30 March 2025 - 3 April 2025*. ACM, 573–588. <https://doi.org/10.1145/3689031.3696070>

[66] Lianmin Zheng, Liangsheng Yin, Zhiqiang Xie, Jeff Huang, Chuyue Sun, Cody Hao Yu, Shiyi Cao, Christos Kozyrakis, Ion Stoica, Joseph E. Gonzalez, Clark W. Barrett, and Ying Sheng. 2023. Efficiently Programming Large Language Models using SGLang. *CoRR* abs/2312.07104 (2023). <https://doi.org/10.48550/ARXIV.2312.07104> arXiv:2312.07104

[67] Yinmin Zhong, Shengyu Liu, Junda Chen, Jianbo Hu, Yibo Zhu, Xuanzhe Liu, Xin Jin, and Hao Zhang. 2024. DistServe: Disaggregating Prefill and Decoding for Goodput-optimized Large Language Model Serving. In *18th USENIX Symposium on Operating Systems Design and Implementation, OSDI 2024, Santa Clara, CA, USA, July 10-12, 2024*, Ada Gavrilovska and Douglas B. Terry (Eds.). USENIX Association, 193–210. <https://www.usenix.org/conference/osdi24/presentation/zhong-yinmin>

[68] Kan Zhu, Yilong Zhao, Liangyu Zhao, Gefei Zuo, Yile Gu, Dedong Xie, Yufei Gao, Qinyu Xu, Tian Tang, Zihao Ye, Keisuke Kamahori, Chien-Yu Lin, Stephanie Wang, Arvind Krishnamurthy, and Baris Kasikci. 2024. NanoFlow: Towards Optimal Large Language Model Serving Throughput. *CoRR* abs/2408.12757 (2024). <https://doi.org/10.48550/ARXIV.2408.12757> arXiv:2408.12757